DOI: 10.1002/ejic.200901214

Hydrothermal Synthesis and Photoluminescence of Hierarchical Lead Tungstate Superstructures: Effects of Reaction Temperature and Surfactants

Xiaohui Guo,*[a,b] Jianping Yang,[a] Yonghui Deng,[a] Hao Wei,[a] and Dongyuan Zhao*[a]

Keywords: Lead / Tungsten / Self-assembly / Surfactants / Morphology

Lead tungstate ($PbWO_4$) crystals with unique hierarchical morphologies have been successfully synthesized in the presence of a triblock copolymer poly(ethylene oxide)-poly(propylene oxide)-poly(ethylene oxide) (EO_{70}-PO_{20}-EO_{70}, P_{123}) under mild hydrothermal conditions. When reaction temperature is changed from 140 to 180 and 220 °C, the as-obtained $PbWO_4$ samples can vary from flat tubular to rod-shaped arrays and complex slabs with porous film texture on their surface. Meanwhile, by using polyvinylpyrolidone (PVP), cetyltrimethylammonium bromide (CTAB), and hydroxycellulose with distinct functional groups as structure-directing agents, $PbWO_4$ samples such as polyhedrons and rods with porous groove texture, as well as tube-shaped aggregate bundles, can be obtained. The optical properties of the as-made $PbWO_4$ samples with various morphologies were examined by photoluminescence (PL) and Raman spectroscopy. Results show that PL of the rod-like arrays and microtube structures is redshifted relative to that of the complex slab sample. In general, the present synthesis route may be extended to prepare other inorganic nanomaterials with special functions.

Introduction

The controlled synthesis of nano- or microsized materials with unique superstructures has become a very active field in materials science. In particular, the dependence of physicochemical properties on the size, shape, orientation, and hierarchical architecture of materials has been attracting much attention in the past decades.[1–4]

There are many synthesis methods for the preparation of nanostructural materials. Laser-assisted catalytic growth (LCG),[5] chemical vapor deposition (CVD),[6] hard templates,[7] electrochemical deposition,[8] and controlled solution growth at elevated temperature or pH are general synthesis routes.[9–10] Moreover, utilization of organic additives,[11] self-assembled organic superstructures,[12] monolayer films,[13] and templates with complex functionalization patterns[14] to control the growth of inorganic materials are also very attractive, since controlled morphologies and architectures can be obtained under nearly natural conditions.[15] Furthermore, inspiration by biomineralization principles has led to the use of synthetic polymers and surfactants as templates or crystal growth modifiers to fabricate novel materials with hierarchical structures.[16]

Recently, nanostructural tungstate materials, for example, $CdWO_4$, $MnWO_4$, $BaWO_4$, $ZnWO_4$, and $SrWO_4$, have attracted much attention, because of their unique photoluminescence features and potential applications in the fields of optics, magnetism, and electronics.[17–19] For example, 1D and 2D $CdWO_4$ thin nanostructures can be formed with the assistance of a block copolymer.[20] $BaWO_4$ nanorods have been obtained by using a simple reverse-micelle soft-template route.[21] In addition, $ZnWO_4$ rods/belts[22] and $MnWO_4$ fibers[23] were synthesized by utilizing a facile hydrothermal/solvothermal method. Notably, strontium tungstate ($SrWO_4$) nanorods with a rough surface were controllably synthesized by a solvothermally mediated microemulsion method.[24] Herein, at a 40:1 molar ratio of water to cetyltrimethylammonium bromide (CTAB) in solution, $SrWO_4$ nanorods with diameters of 150–200 nm and lengths of 3–4 μm were obtained.

As a member of the tungstate family, lead tungstate ($PbWO_4$) is an important inorganic scintillating crystal with tetragonal scheelite-type nano- and microcrystals. It has also been the center of intense focus, because of its technological importance in the field of high-energy physics. It has high density (8.3 $g cm^{-1}$), short decay time (less than 10 ns for a large light output), high irradiation damage resistance

[a] Department of Chemistry, Shanghai Key Laboratory of Molecular Catalysis and Innovative Materials, Advanced Materials Laboratory, Fudan University
Shanghai 200433, China
Fax: +86-21-65641740
E-mail: dyzhao@fudan.edu.cn
[b] Key Laboratory of Synthetic and Natural Functional Molecule Chemistry of the Ministry of Education, The School of Chemical and Materials Science, Northwest University of China
Xi'an 710069, P. R. China
Fax: +86-29-88302604
E-mail: gxh2002@mail.ustc.edu.cn
Supporting information for this article is available on the WWW under http://dx.doi.org/10.1002/ejic.200901214.

(10^7 rad for undoped and 10^8 rad for La-doped $PbWO_4$), and interesting excitonic luminescence, thermoluminescence, and stimulated Raman scattering behavior.[21b,25] Various efforts have been made to develop and prepare lead tungstate materials with specific morphologies. $PbWO_4$ nano- and microcrystals with various morphologies such as rods, spindles, pagodas, and dendrite structures were fabricated through a wet chemical route.[26] Yu et al. synthesized various tungstate nanorods, including $ZnWO_4$, $FeWO_4$, and $MnWO_4$, with different aspect ratios when only changing the pH value in a hydrothermal reaction system.[26b] It was assumed that the solute concentration within the diffusion layer maintains the solubility of a specific crystal face by rapid growth onto or dissolution from the face. The improved diffusive solute flux around the tubular crystals can explain the lateral growth rate and wider size distribution of the nanorods. Nitsch et al. fabricated $PbWO_4$ with a scheelite structure from a gel at low temperature.[27] Geng et al. prepared $PbWO_4$ with spindle and polyhedral structures by a sonochemical method.[28] In contrast, surfactants such as sodium bis(2-ethylhexyl)sulfosuccinate (AOT) and CTAB have been used as soft templates or crystal growth modifiers to synthesize $PbWO_4$ crystals with controllable morphologies.[29] Interestingly, in previous studies, tetragonal $PbWO_4$ microcrystals with unique hierarchical structures were formed by adjusting reaction conditions, including the amount of CTAB, the pH value, and the reaction temperature.[30] Additionally, the controlled synthesis of $PbWO_4$ crystals with dendritic, rod-like, as well as dumbbell structures was performed by a poly(methacrylic acid)-mediated hydrothermal route.[31] It was mentioned that a nucleation-crystallization-oriented assembly growth process governed by poly(methyl methacrylate) (PMMA) could play a key role in forming the distinct morphologies of tungstate. Notably, Yang et al.[32] reported a facile, dextran-directed solution route to synthesize $PbWO_4$ crystals with distinct morphologies. Therefore, it was demonstrated that organic molecules as a soft template can indeed exert significant influence on the morphogenesis of crystals in aqueous solution. Nevertheless, to date there are few papers involved in the morphology-controlled synthesis of $PbWO_4$ crystals with hierarchical superstructures by using triblock copolymers as structure-directing agents.

In this paper, we report for the first time the synthesis of single-crystalline lead tungstates with novel hierarchical superstructures including nanorod arrays, complex slabs, and flat tubular structures by using a versatile triblock copolymer, poly(ethylene oxide)-poly(propylene oxide)-poly(ethylene oxide) ($PEO_{20}PPO_{70}PEO_{20}$, P_{123}) as a crystal modifier under mild hydrothermal conditions. The shape and size of $PbWO_4$ crystals can be readily tuned by altering the reaction temperature and concentration of the triblock copolymer. In addition, we have systematically investigated the photoluminescence (PL) of the as-prepared $PbWO_4$ products with various morphologies. In general, the facile synthesis route that involves no seeds and catalysts may be scaled up and extended further to fabricate other tungstates or inorganic mineral materials with special functions.

Results and Discussion

Interestingly, when the hydrothermal reaction temperature is 140 °C, a kind of half-baked $PbWO_4$ crystal with flat or compressed tubular morphology is obtained in the presence of P_{123} as a structure-directing agent (Figure 1). The maximum length of the tubes is 60 μm (Figure 1b, c). Notably, the inner and outer surface of the tubular samples are all very smooth; the mean diameter of the tubes was measured to be approximately 13 μm (Figure 1d). It should be mentioned that the flat tubular structure of $PbWO_4$ is prepared for the first time by a facile hydrothermal method. In the as-made sample, almost half-baked flat tubular structures can be observed under transmission electron microcopy (TEM), as shown in Figure 2a. The smooth surface of the individual tubes can be observed in the high-magnification TEM image (Figure 2b). After ultrasonic treatment of the as-made tube-like samples for several minutes, some multiple-flake structure blocks are observed (Figure 2d). The average thickness of an individual flake is around 30 nm. The selected area electron diffraction (SAED) measurement for an individual flake (Figure 2c) shows that the flake structures possess good single-crystalline features. It also reveals that the flake crystals have undergone favorable growth along the (011), (201) faces, which agrees well with the results of X-ray diffraction measurements (Figure 2f). Moreover, high-resolution TEM (HRTEM) images of the individual flake structures (Figure 2d, e) show that the crystal spacing of the flake is about 2.46 Å, corresponding to 020 planes, which clearly suggests that the as-obtained flake-like $PbWO_4$ samples are formed with preferable oriented growth along {020} crystal faces.

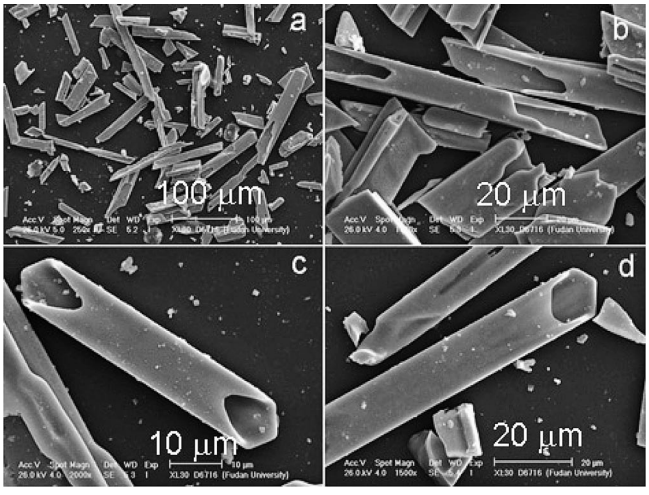

Figure 1. Representative SEM images of the flat-tube-shaped $PbWO_4$ structures with different amplifications (a, b, c, d) obtained at a reaction temperature of 140 °C; $[Pb^{2+}]$ = 20 mmol; $[P_{123}]$ = 12 mM.

As the reaction temperature increases to 180 °C, complex rod-like $PbWO_4$ arrays that are composed of many parallel microrods are observed, and self-stacking occurs along vertical directions (Figure 3a–c). These rod-shaped structures are about several tens of micrometers in length, and the

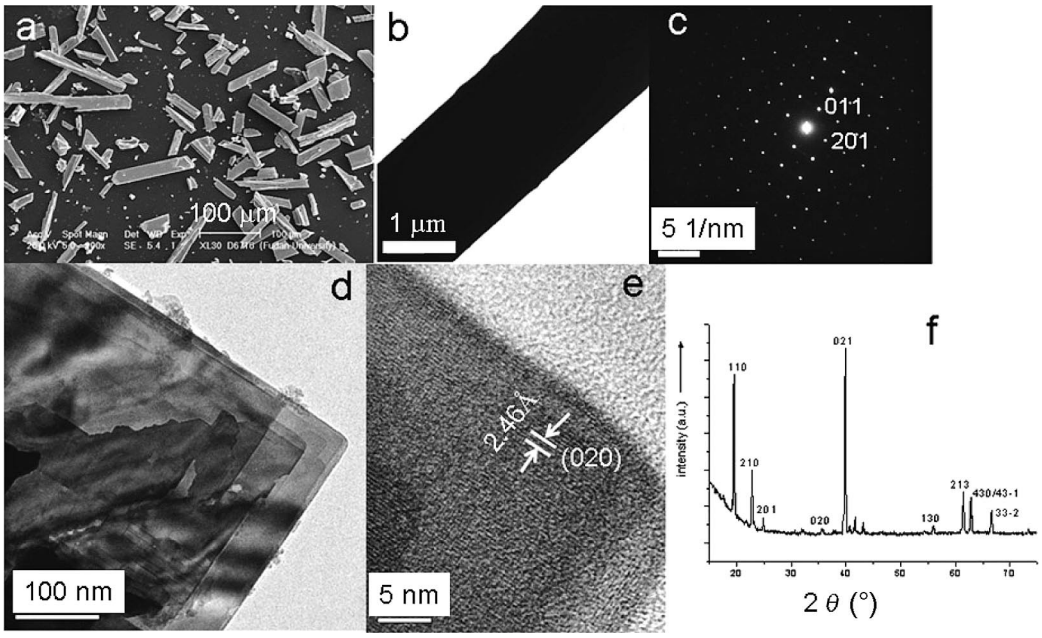

Figure 2. Structural analysis of the typical flat $PbWO_4$ tubes prepared in the presence of P_{123}. (a) the SEM image of the flat tubes; (b) the TEM image of the patch peeled from the flat tubes; (c) the SAED pattern of an individual tube; (d) the TEM image of the patch of the tubular $PbWO_4$ samples; (e) the corresponding HRTEM image taken from Figure 2d; (f) the XRD pattern of the tubular samples. The hydrothermal reaction was carried out at 140 °C for 14 h.

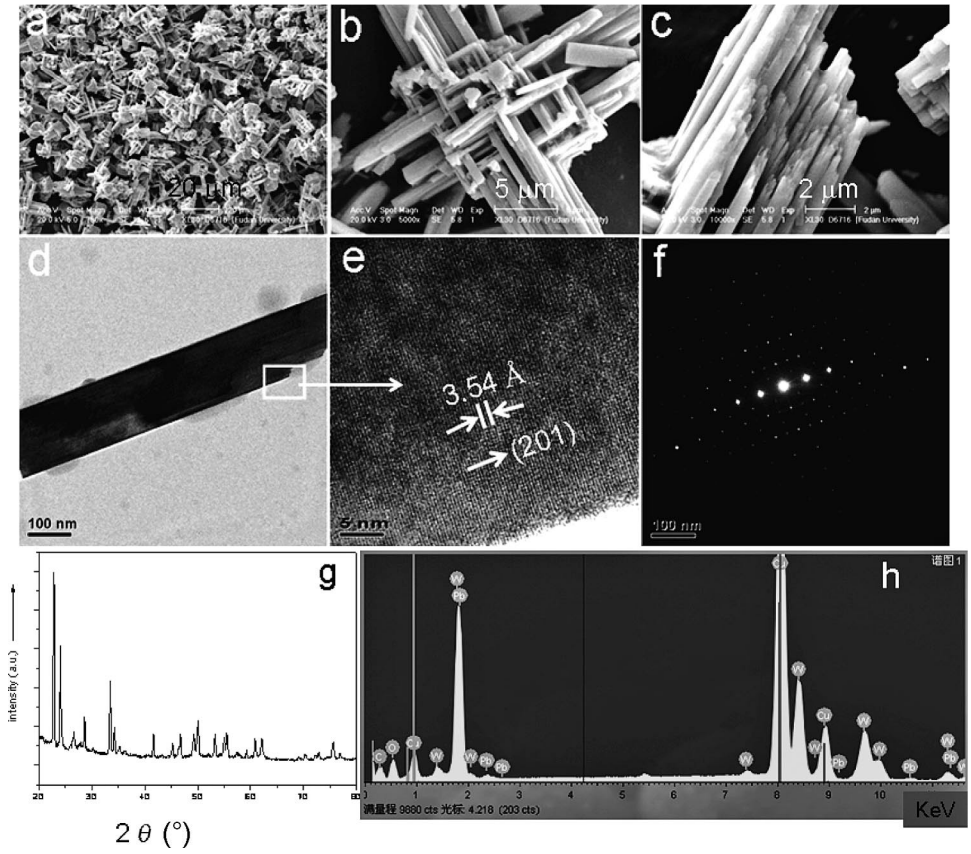

Figure 3. Structural analysis of the representative rod-shaped $PbWO_4$ arrays prepared at a reaction temperature of 180 °C: (a–c) typical SEM images of the rod-like $PbWO_4$ arrays; (d) the TEM image of an individual rod; (e) the HRTEM image of selected area located in the individual rod, as indicated by the arrow coming from Figure 3d; (f) the SAED pattern of the individual rod-shaped $PbWO_4$ structure; (g) the XRD pattern of the rod-shaped $PbWO_4$ product; (h) the EDS pattern of the as-made $PbWO_4$ sample. The synthesis was carried out with $[Pb^{2+}]$ = 20 mmol and $[P_{123}]$ = 12 mM.

typical TEM image of the part of an individual nanorod is shown in Figure 3d. The HRTEM image shows that the as-made $PbWO_4$ sample has a crystal lattice spacing of approximately 3.54 Å, corresponding to 201 crystal planes (Figure 3e), which indicates clearly single-crystalline features. The SAED pattern (Figure 3f) reveals that the as-made lead tungstate sample possesses better single-crystalline features.

The XRD pattern indicates that the as-made $PbWO_4$ samples can be readily indexed as pure monoclinic phases with cell parameters of a = 13.555 Å, b = 4.976 Å, c = 5.561 Å (JCPDS Card Number. 70-0302), which is in good agreement with the SAED result. In addition, the energy-dispersive spectrometry (EDS) result further confirms the composition of the as-made $PbWO_4$, as shown in Figure 3h.

When reaction temperature increases to 220 °C, a complex slab-like $PbWO_4$ structure with a surface coated with a layer of multiple-pore film can be formed (Figure 4a). Interestingly, the slab-like structure is actually composed of many flake units (Figure 4b), and the thickness of an individual flake is measured to be several tens of nanometers. Moreover, the SAED pattern for the individual flake (Figure 4c) clearly shows that the flake structure possesses single-crystalline features. A preferable oriented growth along the (011) and (201) crystal faces is observed. The HRTEM image further confirms the inner crystal structure of the as-made flake sample (Figure 4d). The crystal spacing of the flake is calculated to be about 3.67 Å, which corresponds to the 011 plane of $PbWO_4$. Clearly, the as-made slab products are composed of pure $PbWO_4$ according to the results of EDS analysis (Figure 4e). On the basis of the above results, we conclude that the transformation of the morphology of the as-made $PbWO_4$ samples from tubular to rod-shaped and finally to flake-shaped with increasing reaction temperature can readily occur in our synthesis system.

It has been known that the surfactant templates indeed play an important role in adjusting the morphologies and polymorphs of inorganic nanomaterials.[12,21] Therefore, we further investigated the effect of the templates on the shape and size of the as-prepared $PbWO_4$ samples. It was found that a kind of sixteen-faced polyhedral $PbWO_4$ structure can be obtained in the presence of CTAB (Supporting Information, Figure S1a); its maximum size can be up to 50 μm in length. However, irregular rod-shaped crystals

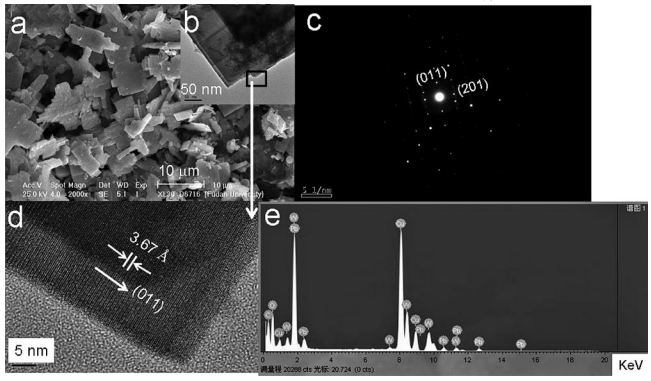

Figure 4. Structural analysis of the typical slab-shaped $PbWO_4$ sample prepared in the presence of P_{123} at a reaction temperature of 220 °C: (a) typical SEM image of the slab-like $PbWO_4$ sample [inset (b) in the top right corner is the TEM image of the patch of slab after ultrasonic treatment]; (c) the SAED image of an individual slab $PbWO_4$ structure; (d) the HRTEM image of an individual $PbWO_4$ flake taken from Figure 4b; (e) the EDS pattern of the as-made $PbWO_4$ sample.

with many structural defects or cavities on their surface are observed when hydroxycellulose is used as a structure-directing agent (Figure S1b). In contrast, a class of tubular aggregate bundles can also be formed in the presence of polyvinylpyrolidone (PVP) (Figure 5). These similar tubular structures seem to be formed by the parallel aggregation and fusion of one into another along the same crystal face direction (Figure 5b). The wall thicknesses and lengths of the microtubes are at least several tens and hundreds of micrometers, respectively (Figure 5c). To the best of our knowledge, the tubular aggregate $PbWO_4$ arrays are also reported for the first time. Our results show that preferable absorption modes between surfactants and the growing crystal faces can effectively modulate the shape, size, and aggregate structures of tungstates. As reported in previous publications,[13] these hierarchical $PbWO_4$ superstructures may be associated with the self-assembly routes facilitated by various reaction conditions. XRD patterns of the above-mentioned $PbWO_4$ samples formed in the presence of three different surfactants (Supporting Information, Figure S2.) can be indexed as pure monoclinic phases according to

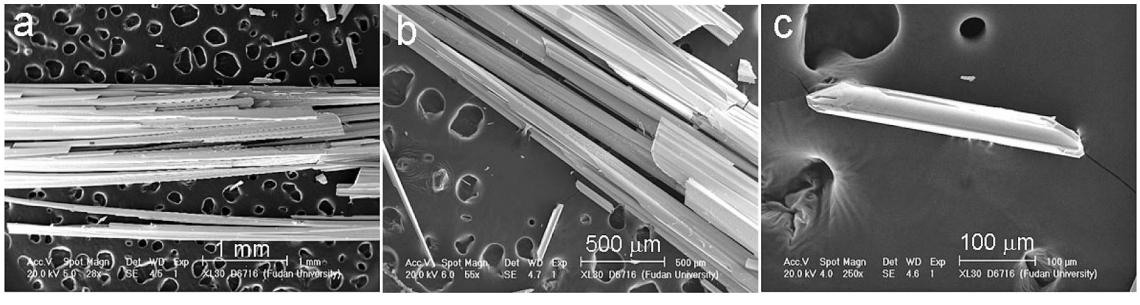

Figure 5. SEM images of the typical tubular $PbWO_4$ bundle-like samples prepared in the presence of PVP as a soft template at 140 °C for 14 h.

standard card data (JCPDS 70-0302), implying a preferable orientation along the (011), (21-1), (020), (021), (32-1) crystal faces. These results confirm that the surfactant templates are critical for modulating the shape and size of the as-made $PbWO_4$ samples.

Possible Formation Mechanism of the Flat Tubular Structures

Considering the above results, we propose a possible formation mechanism for the unique flat tubular nanostructures. At the beginning stage, numerous precursor lead tungstate nuclei are formed in the reaction solution (Figure 6a), and they can interact with triblock copolymers P_{123} by hydrogen bonding and form spherical composite micelle aggregates (Figure 6b). As the reaction proceeds, these micelle aggregates may assume ordered alignments along the direction of the hydrogen interaction of the surfactant (Figure 6c). Afterwards, the larger micelles aggregates can further grow into rod-like intermediates (Figure 6d). The rod-like intermediates can further undergo oriented attachment[21b] and anisotropic self-assembly along 201 crystal planes to form plate or flake structures (Figure 6e, f). During this course, an optional hydrothermal ripening of the $PbWO_4$ flake units can lead to further self-assembly into 2D flat tubular superstructures (Figure 1). The self-organization of the rods into 2D structures induced by hydrothermal treatment is very similar to that reported for $BaWO_4$ and $BaCrO_4$ nanorods,[33] but significantly different from the assembly of the short $BaCrO_4$ and CdSe nanorods, where ribbon-like and vertical rectangular/hexagonal superstructures are formed.[2,34] In addition, because the plate or flake units possess higher surface free energy, the structures can further hierarchically self-assemble and stack to form a tubular superstructure (Figure 6g, h). We believe that the Ostwald ripening process also contributes to the formation of the tube-like lead tungstate.

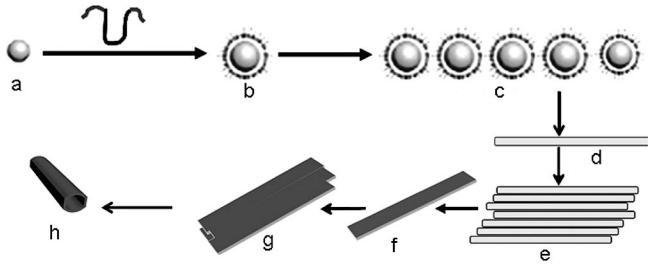

Figure 6. Scheme illustrating the possible formation process of the flat $PbWO_4$ tube-like structures.

Photoluminescence of the $PbWO_4$ Samples

The Raman spectrum of the obtained hierarchical stolzite structure (Figure 7A) shows four bands in the range 100–1000 cm^{-1}. The bands at 813.3 and 426.2 cm^{-1} correspond to the vibration modes ν_3(Bg) and ν_3(Eg), respectively, which are consistent with those reported by Frost and co-workers.[30] However, the two new peaks at 176.1 and 152.8 cm^{-1} were not reported previously.[21] These peaks are not assigned by Ross,[35] but they could be assigned as the translation mode analogous to that of $CdMoO_4$.[31]

PL spectra of the $PbWO_4$ superstructures obtained at different hydrothermal temperatures (Figure 7B) show two main peaks at around 391 and 428 nm. The former is similar to the reported value for the blue emission component;[32,36] however, literature reports state that the as-made $PbWO_4$ nanostructures, including polyhedral, spindle-like, and dot-shaped structures, have their strongest emission peaks at 493, 491, and 483 nm, respectively, indicating their typical green emission feature at 480–500 nm, which may be associated with their smaller dimension.[28] In addition, the synthesized pure $ZnWO_4$ nanorod exhibits a typical blue emission peak at around 488 nm,[26b] indicating the obvious blueshift. The latter case has never been observed previously in bulk stolzite samples. This may be re-

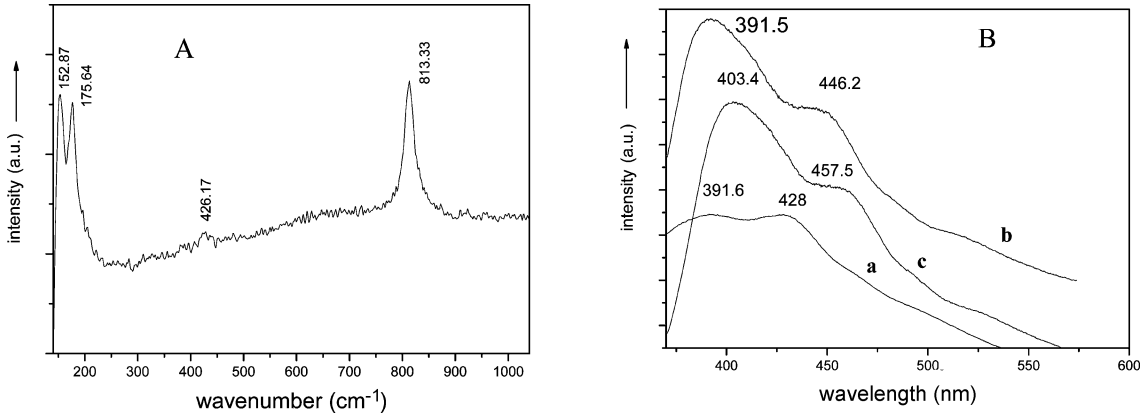

Figure 7. Optical properties of the $PbWO_4$ samples: (A) Raman spectrum; (B) PL spectra at various reaction temperatures [(a) 140, (b) 180, (c) 220 °C].

lated to the surface defects of the crystals, because it was observed in all the samples with different morphologies as their size decreased to the micrometer scale but not in the bulk crystals. In contrast, Liu et al. reported that the as-made $PbWO_4$ with dendritic and peanut-like structures have strong emission peaks at around 580 nm, indicating that the PL performance of tungstates is strongly dependent on the resulting sample morphologies.[21b] Meanwhile, the relative intensities of the two broadening emission peaks seem closely related to the surface/volume ratio.[21a] The slab $PbWO_4$ samples with porous features on surface have the biggest surface/volume ratio, resulting in the highest relative intensity of the peak at 391 nm. In contrast, the relative intensity for flat tubular $PbWO_4$ samples with the smallest surface/volume ratio is the lowest. Notably, very weak size-dependence of PL properties is observed for the samples obtained at a reaction temperature of about 140 °C, suggesting that the sizes are too large, that is, beyond the scope of quantum confinement. Our results show that increasing the reaction temperature can lead to the redshift of the emission from the obtained $PbWO_4$ samples, which is in good agreement with previous reports.[21] This suggests that the superstructures of $PbWO_4$ might influence their optical properties, which could be adopted in fine-tuning the surface-defect-related optical properties of this material.

Conclusions

We have demonstrated a facile hydrothermal approach to prepare $PbWO_4$ crystals with hierarchical superstructures. When the reaction temperature is increased from 140 to 180 °C, and finally to 220 °C, different nanostructures such as flat tube-like and rod-like arrays, as well as complex slabs can be obtained in the presence of P_{123}. Moreover, the length and diameter of a specific tubular structure can reach tens of microns. Using PVP as structure-directing agent, novel tubular aggregate bundle superstructures were formed for the first time. Interestingly, the increase in the hydrothermal reaction temperature led to the redshift of the PL of the three different $PbWO_4$ superstructures. An oriented attachment mechanism is proposed for the formation of the flat hierarchical tube-like structures. Additionally, the feasibility and capability of this approach are worth investigating for other inorganic systems, since it is an efficient and mild solution method with promising advantages over the traditional high-temperature method for the rational design and large-scale production of microcrystal tungstates.

Experimental Section

Synthesis of the Materials: In a typical synthesis, first, WCl_6 was dissolved in absolute anhydrous ethanol; a yellow solution was formed, which then turned dark blue. Subsequently, a mixture of water and hydrochloric acid (20:1 v/v, 70 mL) was added to the above solution with stirring to form a homogeneous dark blue sol solution. The desired amount of triblock copolymer P_{123} and lead acetate (20 mmol) were added into the above sol solution and completely dissolved under strong magnetic stirring at room temperature. The pH value of the solution was adjusted by using hydrochloric acid (HCl) or sodium hydroxide (NaOH), and then the resulting solution was transferred into a Teflon-lined stainless steel autoclave (130 mL). The autoclave was sealed and heated in an oven at varying reaction temperatures (140, 180, and 220 °C) for 14 h. After being naturally cooled down to room temperature, the products were filtered and washed several times with distilled water and absolute ethanol and finally dried in a vacuum at 80 °C for 12 h.

Characterizations: The X-ray diffraction patterns (XRD) were recorded with a Bruker D4 powder X-ray diffractometer by using Cu-K_α radiation (40 kV, 40 mA). Scanning electron microscope (SEM) images were taken with a Philips XL30 electron microscope operating at 20 kV, a thin gold film was sprayed on the sample before the SEM characterization. Transmission electron microscopy (TEM) and selective area electron diffraction (SAED) experiments were conducted with a JEOL-2010 microscope operated at 200 kV. Raman spectra were recorded with a Jobin Yvon (France) LABRAM-1B confocal laser micro-Raman spectrometer at room temperature and an excitation wavelength of 514.5 nm. The PL spectra were recorded with a Fluorolog 3-TAU-P instrument at room temperature with an excitation wavelength of 350 nm.

Supporting Information (see footnote on the first page of this article): SEM images and XRD patterns of lead tungstate crystals formed in the presence of various surfactants.

Acknowledgments

This work was supported by the Natural Science Foundation (NSF) of China (20421303, 20871030, and 20521140450), the State Key Basic Research Program of the PRC (2006CB202502 and 2006CB0N0302), the Shanghai Nanotech Promotion Center (0652nm024), and the Shanghai Education Committee (02SG01). X. Guo thanks the China Postdoctoral Scientific Fund (20070420085) , the research startup fund of Northwest University (No. PR09047), and the Education Ccommittee of Shanxi Province (Grant No. 09JS089) for financial support.

[1] a) S. H. Sun, C. B. Murray, D. Weller, A. Folks, *Science* **2000**, *287*, 1989–1992; b) S. H. Sun, H. Zeng, D. B. Robinson, *J. Am. Chem. Soc.* **2004**, *126*, 273–279.
[2] X. G. Peng, L. Manna, W. D. Yang, J. Wickham, E. Schatz, A. Kadavanich, A. P. Aplivisators, *Nature* **2000**, *404*, 59–61.
[3] R. Jin, Y. Cao, C. A. Mirkin, K. L. Kelly, G. C. Schatz, J. G. Zheng, *Science* **2001**, *294*, 1901–1903.
[4] T. Hyeon, S. S. Lee, J. Park, Y. Chung, N. H. Bin, *J. Am. Chem. Soc.* **2001**, *123*, 12798–12801.
[5] a) Y. Sun, Y. Xia, *Science* **2002**, *298*, 2176–2179; b) Y. G. Sun, B. T. Mayers, Y. Xia, *Nano Lett.* **2002**, *2*, 481–485.
[6] a) F. Caruso, M. Spasova, A. Susha, M. Giersig, R. A. Caruso, *Chem. Mater.* **2001**, *13*, 109–116; b) T. Hyeon, *Chem. Commun.* **2003**, 927–934.
[7] a) A. Ulman, *Chem. Rev.* **1996**, *96*, 1533; b) S. M. Veronica, C. D. Miguel, *Adv. Mater.* **2007**, *19*, 4131–4144.
[8] M. C. K. Wiltshire, J. B. Pendry, I. R. Young, D. J. Larkman, D. J. Gilderdale, J. V. Hajnal, *Science* **2001**, *291*, 849–851.
[9] C. K. Lin, Y. Li, M. Yu, P. Yang, J. Lin, *Adv. Funct. Mater.* **2007**, *17*, 1459–1465.
[10] X. L. Hu, J. C. Yu, J. M. Gong, Q. Li, G. S. Li, *Adv. Mater.* **2007**, *19*, 2324–2329.
[11] Y. Xiong, Z. Li, X. Li, B. Hu, Y. Xie, *Inorg. Chem.* **2004**, *43*, 6540–6542.
[12] I. Cesar, A. K. Jose, G. Martinez, M. Gratzel, *J. Am. Chem. Soc.* **2006**, *128*, 4582–4583.
[13] L. S. Zhong, J. S. Hu, H. P. Liang, A. M. Cao, W. G. Song, L. J. Wan, *Adv. Mater.* **2006**, *18*, 2426–2431.

[14] H. Q. Cao, G. Z. Wang, L. Zhang, L. Liang, S. C. Zhang, X. R. Zhang, *ChemPhysChem* **2006**, *7*, 1897–1901.
[15] K. Woo, H. J. Lee, J. P. Ahn, Y. S. Park, *Adv. Mater.* **2003**, *15*, 1761–1764.
[16] L. Vayssieres, C. Sathe, S. M. Butorin, D. K. Shuh, J. Nordgren, J. K. Guo, *Adv. Mater.* **2005**, *17*, 2320–2323.
[17] J. Chen, L. N. Xu, W. Y. Li, X. L. Guo, *Adv. Mater.* **2005**, *17*, 582–586.
[18] P. Lecoq, I. Dafinei, E. Auffray, M. V. Korzhik, V. B. Pavlenko, A. Fedorov, A. N. Annencov, V. L. Kostyllev, V. D. Ligun, *Nucl. Instrum. Methods Phys. Res. Sect. A* **1995**, *365*, 291–298.
[19] A. Kaminskii, H. J. Eichler, K. Ueda, N. V. Klassen, B. S. Redkin, L. E. Li, J. Findeisen, D. Jaque, J. Garcia-Sole, J. Fernandez, R. Balda, *Appl. Opt.* **1999**, *38*, 4533–4547.
[20] C. H. An, K. B. Tang, G. Z. Shen, C. R. Wang, Y. T. Qian, *Mater. Lett.* **2002**, *57*, 565–568.
[21] a) S. H. Yu, M. Antonietti, H. Cölfen, M. Giersig, *Angew. Chem. Int. Ed.* **2002**, *41*, 2356–2360; b) B. Liu, S. H. Yu, L. J. Li, Q. Zhang, F. Zhang, K. Jiang, *Angew. Chem. Int. Ed.* **2004**, *43*, 4745–4750.
[22] X. L. Hu, Y. J. Zhu, *Langmuir* **2004**, *20*, 1521–1523.
[23] K. Nitsch, M. Nikl, M. Rodova, S. Santucci, *Phys. Status Solid A* **2000**, *179*, 261–265.
[24] L. Sun, Q. Guo, X. Wu, S. Luo, W. Pan, K. Huang, J. Lu, L. Ren, M. H. Cao, C. W. Hu, *J. Phys. Chem. C* **2007**, *111*, 532–537.
[25] a) R. L. Penn, J. F. Banfield, *Geochim. Cosmochim. Acta* **1999**, *63*, 1549–1557; b) R. L. Penn, J. F. Banfield, *Science* **1998**, *281*, 969–971.
[26] a) Z. Y. Tang, N. A. Kotov, M. Giersig, *Science* **2002**, *297*, 237–240; b) S. H. Yu, B. Liu, M. S. Mo, J. H. Huang, X. M. Liu, Y. T. Qian, *Adv. Funct. Mater.* **2003**, *13*, 639–647.
[27] K. Nitsch, M. Nikl, M. Rodova, S. Santucci, *Phys. Status Solidi A* **2000**, *1*, 261–264.
[28] J. Geng, J. J. Zhu, H. Y. Chen, *Cryst. Growth Des.* **2006**, *6*, 321–326.
[29] Y. Ma, L. Qi, J. Ma, H. Cheng, *Cryst. Growth Des.* **2004**, *4*, 351–356.
[30] M. Crane, R. L. Frost, P. A. Williams, J. T. Kloprogge, *J. Raman Spectrosc.* **2002**, *33*, 62–65.
[31] J. G. Yu, X. F. Zhao, S. W. Liu, M. Li, S. Mann, D. H. L. Ng, *Appl. Phys. A: Mater. Sci. Process* **2007**, *87*, 113–120.
[32] J. H. Yang, C. H. Lu, H. Su, J. M. Ma, M. Cheng, L. M. Qi, *Nanotechnology* **2008**, *3*, 035608.
[33] F. Kim, S. Kwan, J. Akana, P. D. Yang, *J. Am. Chem. Soc.* **2001**, *123*, 4360–4361.
[34] M. Li, H. Schnablegger, S. Mann, *Nature* **1999**, *402*, 393–395.
[35] S. D. Ross, *Inorganic Infrared and Raman Spectra*, McGraw-Hill, Maidenhead, **1972**.
[36] a) K. Polak, M. Nikl, K. Nitsch, M. Kobayashi, M. Ishii, Y. Usuki, O. Jarolimek, *J. Lumin.* **1997**, *72*, 781–783; b) M. Nikl, P. Strakova, K. Nitsch, V. Petricek, V. Mucka, O. Jarolimek, J. Novak, P. Fabeni, *Chem. Phys. Lett.* **1998**, *291*, 300–304.

Received: December 16, 2009
Published Online: March 4, 2010

